[9] de Dios Ruiz J, Martinez FL, Hinojosa J. Optimization of chirped and tapered microstrip Koch fractal electromagnetic bandgap structures for improved low-pass filter design. *IET Microwav Antenna Propagat.* 2015;9(9):889–897.

[10] Huang SY, Lee YH. Tapered daul-plane compact electromagnetic bandgap microstrip filter structure. *IEEE Trans Microw Theor Tech.* 2005;53(9):2656–2664.

[11] Sanjeeva Reddy BR, Vakula D. Compact zigzag-shaped-slit microstrip antenna with circular defected ground structure for wireless applications. *IEEE Antenna Wirel Propagat Lett.* 2015;14:678–681.

[12] Kumar C, Guha D. Reduction in cross-polarized radiation of microstrip patches using geometry-independent resonant-type defected ground structure (DGS). *IEEE Trans Antenna Propagat.* 2015;63(6):2767–2772.

[13] Zhou H, Mao J. Miniaturized tapered EBG structure with wide stopband and flat passband. *IEEE Antenna Wirel Propagat Lett.* 2012;11:314–317.

[14] de Dios Ruiz J, Martinez FL, Hinojosa J. Novel compact wideband EBG structure based on tapered 1-D koch fractal patterns. *IEEE Antenna Wirel Propagat Lett.* 2011;10:1104–1107.

[15] Alit Apriyana AA, Zhang YP, Chang JS. Single-pole multiple-throw switches with defected ground structure low-pass filter. *IET Microwav Antenna Propagat.* 2014;8(14):1241–1249.

How to cite this article: Rong H, Wang Q, Chen S, Cao Y, Tian H. Wide stopband miniaturized "I"-typed EBG with DGS. *Microw Opt Technol Lett.* 2017;60:44–50. https://doi.org/10.1002/mop.30910

Received: 19 June 2017

DOI: 10.1002/mop.30907

SIW-induced dualmode dualband loop antenna: A new design insight and guideline

Suvadeep Choudhury | **Akhilesh Mohan** | **Debatosh Guha**

Indian Institute of Technology, Kharagpur, India

Correspondence
Akhilesh Mohan, Indian Institute of Technology, Kharagpur, India.
Email: am@ece.iitkgp.ernet.in

Abstract

A quasi-omnidirectional printed antenna has been developed using Substrate Integrated Waveguide (SIW) technology. The radiating element is realized from a concept of segmented circular SIW cavity through repetitive bifurcation by magnetic walls and also by reshaping its ground plane. The conjecture and design insight have been discussed and demonstrated indicating matching bandwidth of 7.7% (3.49–3.77 GHz for TM_{010}-like mode) and 21.3% (5.08–6.29 GHz for TM_{020}-like mode). As much as 2 dBi gain with nonuniform quasi-omnidirectional radiation patterns has been experimentally documented. This work should find applications in compact wireless transceivers operating in WiMAX (IEEE 802.16) and WLAN (IEEE 802.11) bands.

KEYWORDS

current loop, magnetic wall, quasi-omnidirectional radiation, sixty-fourth mode substrate integrated waveguide, SIW-induced

1 | INTRODUCTION

The rapid development in wireless communication systems has prompted the need of portable as well as multifunctional devices. Commonly known techniques involve the use of high permittivity substrates/superstrates,[1,2] magneto-dielectric materials,[3] and capacitive loading.[4] Multiband design introduces slots,[5,6] stub,[7] and metamaterials.[8] But most of them are poor in efficiency and also their size reduction is limited to $\sim\lambda_0/8$.

A different approach using substrate integrated waveguide (SIW) technology was explored very recently in Ref. [9]. There, a small geometry bearing the 64^{th} mode, ie, $1/64^{th}$ section of a circular parch was realized as a SIW-variant of a planar monopole. That demonstrated quasi-omnidirectional radiations occurring at its fundamental resonant mode.

The SIW monopole[9] shows few limitations: (i) the ground plane width ($\sim 0.3\lambda$) is 6 times larger than that of the primary radiator; (ii) its higher order resonances do not help in effective antenna radiations.

In this paper, we have tried to alleviate all these shortcomings by replacing the large ground plane by a sleek configuration of equal width of the $1/64^{th}$ element which indeed transforms the planar monopole to a loop-like structure. This actually helps in improving the modal characteristics where two successive modes have been successfully employed in this design in realizing dualmode dualband operation with quasi-omnidirectional radiation patterns.

This investigation embodies systematic studies of the modal fields leading to a complete design insight. A complete antenna design operating at two different wireless bands: 3.49–3.77 GHz (WiMAX-IEEE 802.16) and 5.08–6.29 GHz (WLAN-IEEE 802.11) have been presented and experimentally verified. The principle of operation has been studied and identified as (i) TM_{010}-like mode (3.49–

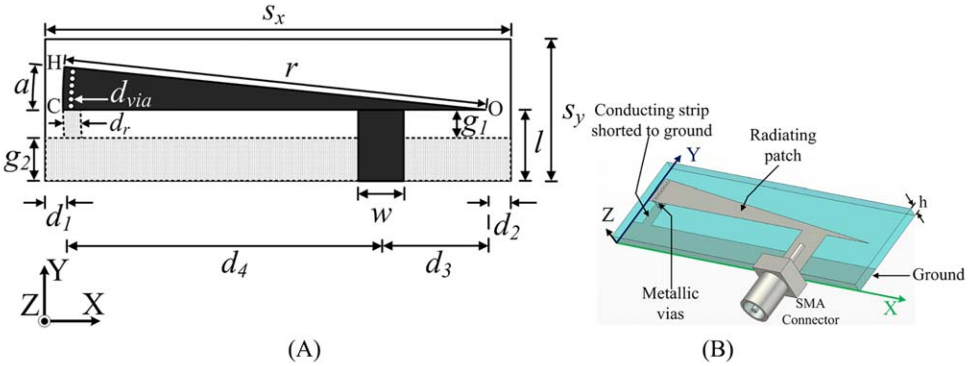

FIGURE 1 Configuration of the proposed SFMSIW-induced antenna: (A) top and bottom views (bottom view has been shown dotted) and (B) perspective view. [Color figure can be viewed at wileyonlinelibrary.com]

3.77 GHz) which turns the antenna to a full-wavelength loop and (ii) TM_{020}-like mode (5.08–6.29 GHz). As much as 7.7% matching bandwidth for the first mode and 21.3% bandwidth for the second radiating mode have been experimentally demonstrated showing about 2 dBi gain. This study helps us also in proposing a comprehensive design guideline for any practicing engineer intending to develop small wireless transceiver systems.

2 | SIW-INDUCED LOOP AND CHARACTERISTICS

The proposed antenna configuration is shown in Figure 1. It is actually a 1/64th section of circular SIW ($a = 2\pi r/64$) with a sleek ground plane having width $g_2 \approx a$. The basic philosophy of realizing such a section by introducing magnetic walls was discussed in Ref. [9]. It would be relevant to note that we cannot increase the number of segments infinitely. The open side walls then become too close to each other causing interaction with the adjacent fringing fields and destroying the basic modal characteristics.

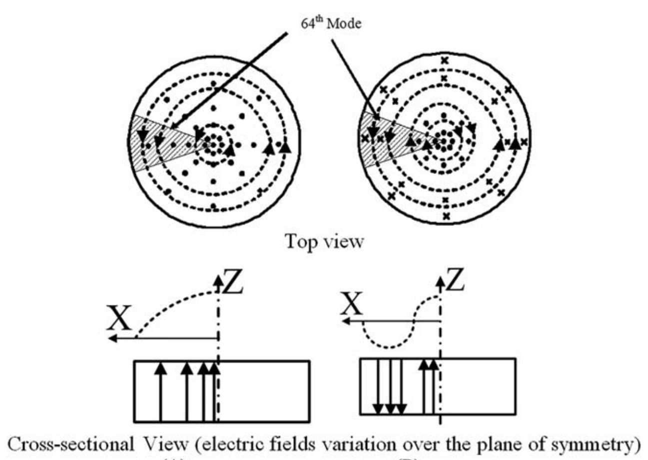

FIGURE 2 Magnitude of total field distribution of circular SIW cavity in (A) TM010 mode and (B) TM020 mode (——: E field, -----: H field)[10]

The structure now represents a loop-like quasi-planar structure with loop-perimeter $\approx 2d_4 + 2g_1$. The gap parameter g_1 is kept small ($g_1 \leq g_2$). Copper vias of diameter d_{via}, indicated by six white dots on the black metal surface, are vertically inserted and soldered with an extended ground plane ($d_r \approx 2 \times d_{via}$) on the reverse side. The grounded strip maintains the curvature of the shorted electric wall. In this design, the antenna dimension is made as compact as possible and therefore the ground plane extension has been deliberately reduced to $d_1 \approx d_2 \approx 0.05 \times r$.

In a 1/64th loop configuration, we have conjectured two TM^Z modes (TM_{010} and TM_{020}) as shown in Figure 2. Thus, it can be segmented theoretically by n number of quasi-magnetic walls passing through the center. The resonant frequency of TM_{nm0} mode is given by:

$$f|_{TM_{nm0}}(\text{conventional}) = \frac{1}{\pi\sqrt{\mu\varepsilon}}\left(\frac{p_{nm}}{d}\right) \quad (1)$$

where $d = 2r$, r being the radius of the cavity and p_{nm} is the mth zero of Bessel's function of order n.

Now, when we segregate the cavity into quarter (1/4th section) and higher modes, its radius is found to determine the operating frequency as,

$$f|_{TM_{nm0}}(\text{modified}) \approx \frac{1}{\pi\sqrt{\mu\varepsilon}}\left(\frac{p_{nm}}{r}\right) \quad (2)$$

The S_{11} characteristics of the SIW loop depicted in Figure 3A indicates distinct dual resonances occurring around 3.55 and 5.8 GHz where the first one corroborates the resonance obtained in Ref. [9]. The loop-length ($\approx 2d_4 + 2g_1 \approx 80$ mm) is in close approximation with λ_1 ($\approx$84 mm, 1st resonance) and 1.5 * λ_2 ($\approx$78 mm, 2nd resonance). Now an eigen-mode analysis is presented in Table 1 to verify the conjecture and identify the modes. For the analysis using,[11] the structure was

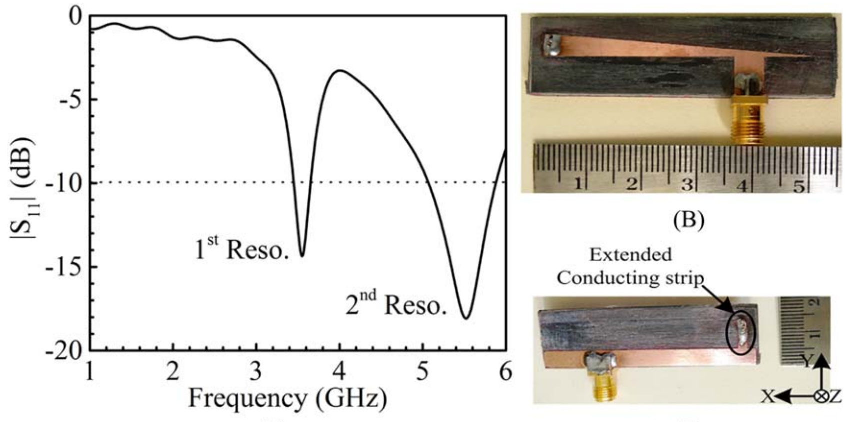

FIGURE 3 (A) Simulated reflection coefficient of 64th mode SIW without ground plane backing; Fabricated prototype (B) top view and (C) bottom view (optimized dimensions: Sx = 55 mm, Sy = 16.2 mm, r = 48 mm, d_{via} = 0.6 mm, g_1 = 3.5 mm, g_2 = 4.7 mm, d_1 = d_2 = 3.5 mm, d_3 = 11.75 mm, d_4 = 36.25 mm, w = 5.2 mm, l = 8.2 mm, h = 1.57 mm, ε_r = 2.2). [Color figure can be viewed at wileyonlinelibrary.com]

enclosed in an air box with electric walls. A vertical space 5h and lateral space 0.6r were provided. Electric fields in column 1 (SIW cavity with full ground plane) closely corroborate TM_{010} and TM_{020} modes of Figure 2. The field portrays in column 2 (truncated small ground plane) ensure the same modal nature as in column I and thus help in working with these modes in SIW-induced loop type antenna.

But the SIW-loop is different from a traditional loop, ie, Figure 4A. A comparison of their S_{11} (Figure 4B) shows that the 1st resonance mutually corroborate but the 2nd ones fail. The radiations of the 2nd resonance also significantly differ from each other: SIW-loop provides 1.9 dBi gain which for traditional loop keeps only 0.2 dBi.

3 | EXPERIMENTS AND VALIDATION

A prototype has been fabricated on Rogers RT/Duroid 5880 by our in-house facilities such as MITS 21T Precision Machine. The top and bottom views of the prototype are shown in Figure 3B,C, respectively. Rosenberger's 32K101-400L5 SMA connector has been used to feed the antenna. It was measured using Agilent's E5071C ENA Series Network Analyzer and a semi-automated Anechoic Chamber. Some representative results are presented in here.

The simulated and measured i_{11} values are shown in Figure 5A. The measurements are found to closely agree with the simulated results. Measured −10 dB bandwidth of 7.7% (3.49–3.77 GHz) for TM_{010}-like mode and 21.3% (5.08–6.29 GHz) for TM_{020}-like mode exactly follow the simulated predictions.

Its principal plane radiation patterns obtained at 3.54 and 5.5 GHz are shown in Figures 6 and 7, respectively. As conjectured, both resonant modes produce nonisotropic omnidirectional radiations. The concept of loop makes considerable

TABLE 1 Eigen-mode performance newly conceived SIW loop compared with conventional SIW cavity

Full ground plane (gray shade) and electric field	Proposed fractional ground plane (gray shade) and electric field
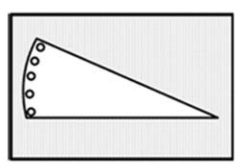	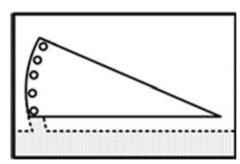
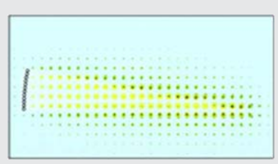 3.52 (TM010)	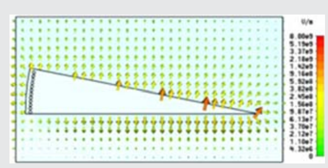 3.5 (TM010- like)
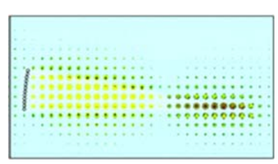 5.60 (TM020)	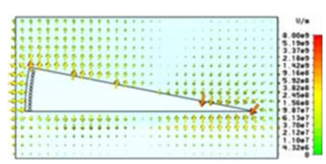 5.58 (TM020- like)

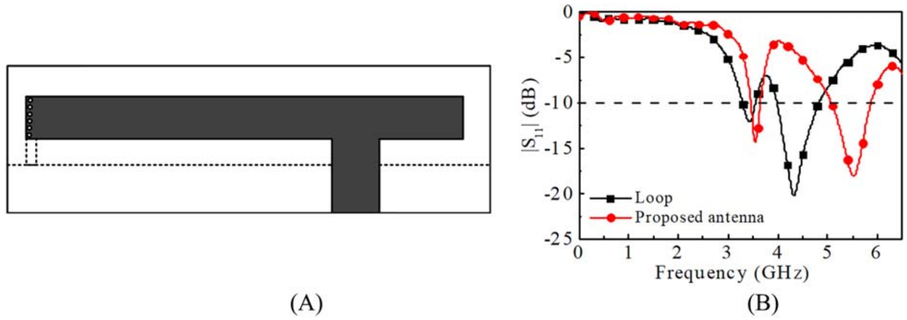

FIGURE 4 Traditional loop antenna: (A) top view (ground boundary shown dotted) and (B) simulated reflection coefficient of a traditional loop compared with the proposed antenna. [Color figure can be viewed at wileyonlinelibrary.com]

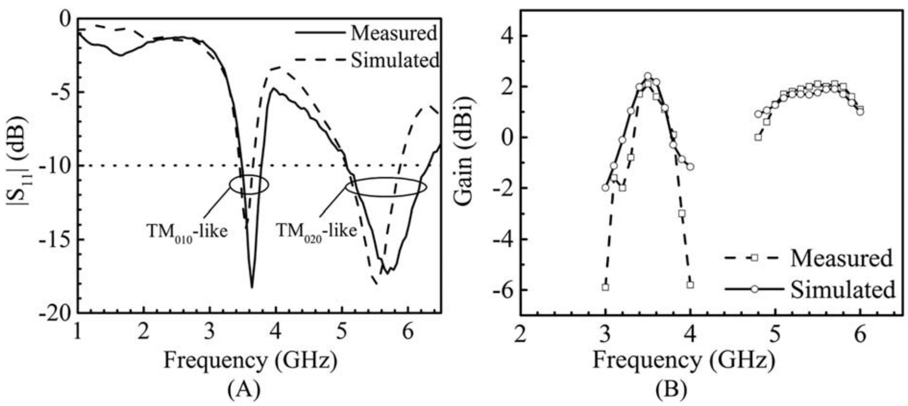

FIGURE 5 Simulated and measured results of the proposed antenna: (A) reflection coefficient and (B) gain

change in the radiation patterns compared to those of[9] treated as SIW-monopole. The measurements are found to follow the simulated predictions, but a lack of close mutual correspondence is observed, especially in Figure 7A,B. The main reason is the lack of pattern symmetry in radiation fields and its rapidly changing nature with the angles as revealed from the 3D portrays in Figure 8. Therefore, even a very little or nominal misalignment in the measurement setup would cause considerable deviation from the theoretical data and that is observed in our case. Their cross-polar levels are over 10 dB down compared to the copolar peak levels. Linear polarization of the proposed antenna is confirmed. The peak gain varies from 2.1 to 1.9 dBi. A study has been depicted in Figure 5B based on simulated and measured data at its two operating bands.

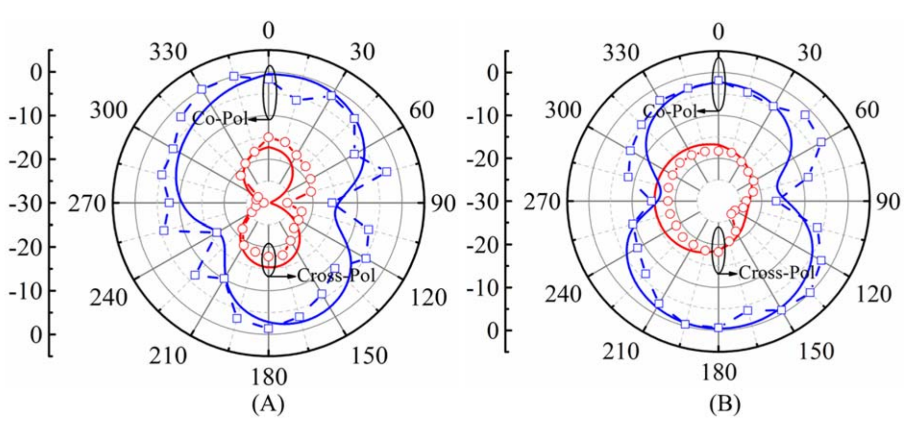

FIGURE 6 Measured copolarization and cross-polarization patterns in (A) xz-planes and (B) yz-planes at 3.54 GHz (——: Simulated, ------: Measured). [Color figure can be viewed at wileyonlinelibrary.com]

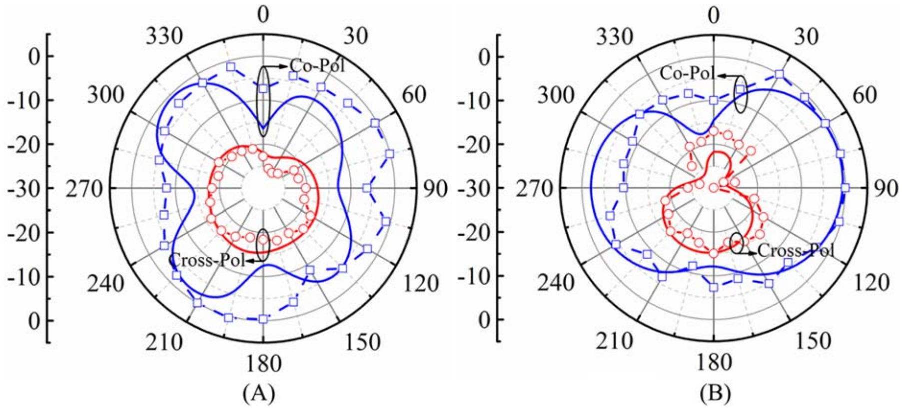

FIGURE 7 Measured copolarization and cross-polarization patterns in (A) xz-planes and (B) yz-planes at 5.5 GHz (——: Simulated, ------: Measured). [Color figure can be viewed at wileyonlinelibrary.com]

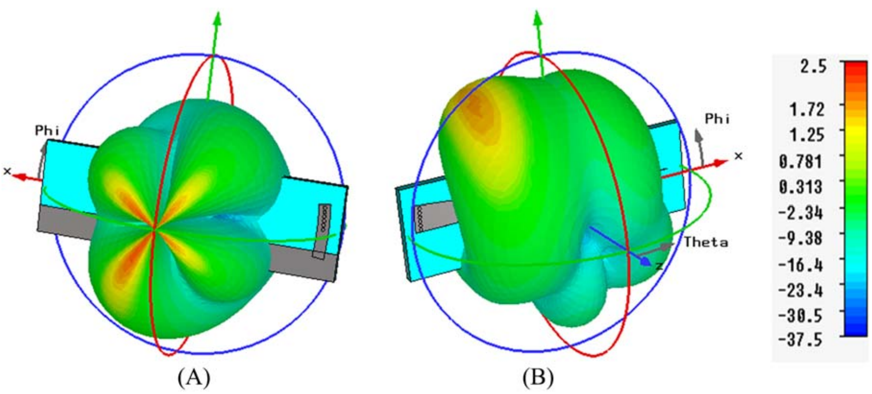

FIGURE 8 Simulated 3D radiation patterns for (A) 1st resonance, and (B) 2nd resonance. [Color figure can be viewed at wileyonlinelibrary.com]

The radiation efficiency of the antenna has been measured using Wheeler cap technique and its theoretical calculation can be seen from Ref. [12]. The measured results have been obtained by averaging 15 samples (S_{11} values under different boundary conditions) in each case and are 76.5% (Simu: 77.6%) and 79.3% (Simu: 79.51%) for the 1st and 2nd modes, respectively, which closely corroborate the simulated predictions.

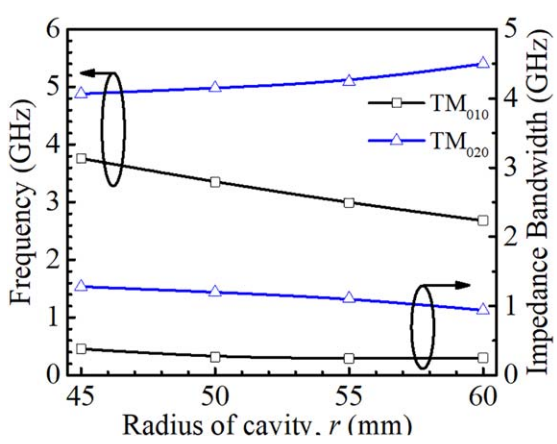

FIGURE 9 Effects of varying the radius *r* in the proposed antenna. [Color figure can be viewed at wileyonlinelibrary.com]

4 | DESIGN GUIDELINES

This study helps us in formulating few necessary steps to design the proposed antenna for any practical applications. They are briefly stated as follows:

1. Low loss thin PTFE substrate[13] with typical values of ε_r 2.2–2.3 and thickness = 1–2 mm is recommended. Also, the h/r ratio should be <2 to operate with TM_{010} mode,[10] which is our mode of interest.
2. An estimation for r can be determined for TM_{010} mode to resonate at a given frequency say $f|_{TM_{010}}$ (following Equation 2). With this r value, an eigenmode analysis needs to be performed to have a primary knowledge of the modes in a true cavity.
3. The parameters relating to the metallic vias may be determined as:[14]: $d_{via}/\lambda_0 < 0.1$, $d_{gap} < 2 \times d_{via}$, where d_{gap} is

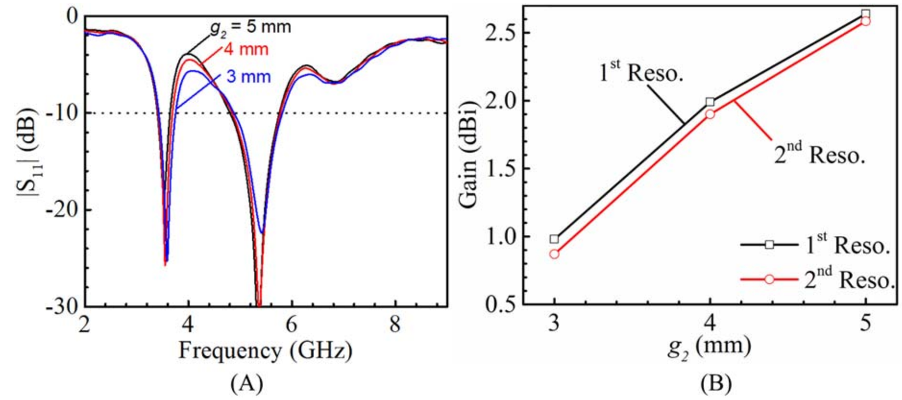

FIGURE 10 Effect of parameter g_2 on the (A) S_{11} response and (B) gain of the proposed antenna. [Color figure can be viewed at wileyonlinelibrary.com]

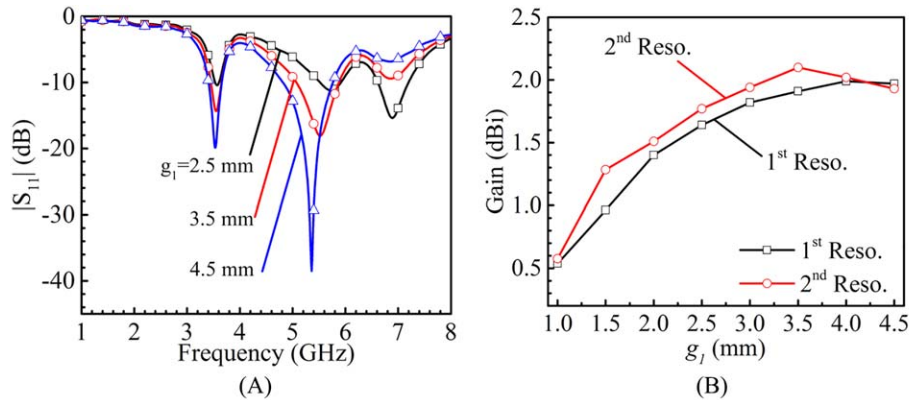

FIGURE 11 Effect of parameter g_1 on the (A) S_{11} response and (B) gain of the proposed antenna. [Color figure can be viewed at wileyonlinelibrary.com]

the via-to-via center separation, and λ_0 is the resonant wavelength for the first resonance.

4. An increase in r decreases d_3/d_4 ratio pushing the feed toward O. The field being maximum near O, experiences gradually increased perturbation as r increases. This perturbation would affect the 2nd mode predominantly and cause an increase in modal separation as experienced in Ref. [15]. Such an increase in modal separation is also evident in Figure 9.

5. The ground plane dimensions:
   - $g_2 \approx a$, and $g_1 \approx 0.75 \times g_2$. The effect of g_2 on the impedance and gain values is examined in Figure 10A, B. Wider g_2 values help in improving both gain and impedance matching. G_1 controls fringing field or coupling effects and influences the input impedance and gain as examined in Figure 11. Moderate value of $g_2 = a = 4.7$ mm and $g_1 = 3.5$ mm are recommended to be an optimum choice.

TABLE 2 Comparison of performances of the proposed antenna with earlier designs

Type of Antenna	Dimension (×λ02)	Matching BW (%)	Gain (dBi)	Radiation Pattern
SIW[16]	0.414	4.8/21.6	4.12/∼6	Broad/Broad
SIW[17]	0.448	1.55	5.9	Broad
Metamat.[18]	0.291	3	0.79	Omni
PIFA[19]	0.291	24.5	5	Broad
This work	0.1216	7.7/21.3	2.1/2.3	Omni/Omni

Broad: Broadside, Omni: Omnidirectional.

- Extended ground-strip should follow the curvature of the section HC and $d_r \approx 2 \times d_{via}$.

6. The feed dimensions:
   - Width w needs to be determined using any standard microstrip line calculator available online.

The feed location d_3 from O is $\approx 0.25 \times r$ which may need fine tuning to obtain 50Ω impedance matching.

5 | CONCLUSION

This work presents a new class of miniaturized "hybrid" SIW antenna, which can be used to obtain quasi-omnidirectional radiation patterns. A relative comparison of the present antenna with some earlier SIW,[16,17] metamaterial based miniaturized antennas[18] and PIFA[19] are presented in Table 2. This is self-explanatory revealing its suitability and superiority in terms of the operating bandwidth, size, and gain.

ORCID

Akhilesh Mohan http://orcid.org/0000-0002-5687-6218

REFERENCES

[1] Hwang Y, Zhang YP, Zheng GX, Lo TK. Planar inverted- F antenna loaded with high permittivity material. *Electron Lett.* 1995;31:1710–1712.

[2] Lo TK, Ho CO, Hwang Y, Lam EKW, Lee B. Miniature aperture-coupled microstrip antenna of very high permittivity. *Electron Lett.* 1997;33:9–10.

[3] Lee J, Heo J, Lee J, Han Y. Design of small antennas for mobile handsets using magneto-dielectric material. *IEEE Trans Antennas Propag.* 2012;60:2080–2084.

[4] Rowell CR, Murch RD. A capacitively loaded PIFA for compact mobile telephone handsets. *IEEE Trans Antennas Propag.* 1997;45:837–842.

[5] Moosazadeh M, Kharkovsky S. Compact and small planar monopole antenna with symmetrical L- and U-shaped slots for WLAN/WiMAX applications. *IEEE Antennas Wireless Propag Lett.* 2014;13:388–391.

[6] Kim JW, Jung TH, Ryu HK, Woo JM, Eun CS, Lee DK. Compact multiband microstrip antenna using inverted-L- and T-shaped parasitic elements. *IEEE Antennas Wireless Propag Lett.* 2013;12:1299–1302.

[7] Cao YF, Cheung SW, Yuk TI. A multiband slot antenna for GPS/WiMAX/WLAN systems. *IEEE Trans. Antennas Propag.* 2015;63:952–958.

[8] Huang H, Liu Y, Zhang S, Gong S. Multiband metamaterial-loaded monopole antenna for WLAN/WiMAX applications. *IEEE Antennas Wireless Propag Lett.* 2015;14:662–665.

[9] Choudhury S, Mohan A. Electrically small 64th-mode substrate-integrated waveguide monopole antenna. *Electron Lett.* 2016;52:580–581.

[10] Harrington RF. *Time Harmonic Electromagnetic Fields*, New York: McGraw-Hill; 1961.

[11] [Online]. Available: http://www.cst.com/.

[12] Guha D, Banerjee A, Kumar C, Antar YMM. Higher order mode excitation for high-gain broadside radiation from cylindrical dielectric resonator antennas. *IEEE Trans Antennas Propag.* 2012;60:71–77.

[13] Balanis CA. *Antenna Theory Analysis and Design*, 3rd ed. New York, NY, USA: Wiley; 2005.

[14] Dashti H, Neshati MH. Development of low-profile patch and semi-circular SIW cavity hybrid antennas. *IEEE Trans Antennas Propag.* 2014;62:4481–4488.

[15] Wong SW, Feng SF, Zhu L, Chu QX. Triple- and quadruple-mode wideband bandpass filter using simple perturbation in single metal cavity. *IEEE Trans Microwave Theory Tech.* 2015;43:3416–3424.

[16] Jin C, Li R, Alphones A, Bao X. Quarter-mode substrate integrated waveguide and its application to antennas design. *IEEE Trans Antennas Propag.* 2013;61:2921–2928.

[17] Sam S, Lim S. Electrically small eighth-mode substrate-integrated waveguide (EMSIW) antenna with different resonant frequencies depending on rotation of complementary split ring resonator. *IEEE Trans Antennas Propag.* 2013;61:4933–4939.

[18] Zhu J, Eleftheriades GV. Compact transmission-line metamaterial antenna with extended bandwidth. *IEEE Antennas Wireless Propag Lett.* 2009;8:295–298.

[19] Chattha HT, Nasir M, Abbasi QH, Huang Y, AlJa'afreh SS. Compact low-profile dual-port single wideband planar inverted-f MIMO antenna. *IEEE Antennas Wireless Propag Lett.* 2013;12:1673–1675.

How to cite this article: Choudhury S, Mohan A, Guha D. SIW-induced dualmode dualband loop antenna: A new design insight and guideline. *Microw Opt Technol Lett.* 2017;60:50–56. https://doi.org/10.1002/mop.30907

Received: 22 June 2017

DOI: 10.1002/mop.30909

Dual-/triple-wideband microstrip bandpass filter using independent triple-mode stub-loaded resonator

Z. J. Wang | **C. Wang** | **N. Y. Kim**

RFIC Center, Kwangwoon University, Seoul 139-701, Korea